Thin–Walled Structures 192 (2023) 111140

Contents lists available at ScienceDirect

Thin-Walled Structures

journal homepage: www.elsevier.com/locate/tws

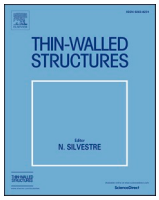

Full length article

Equivalent geometrical imperfections for local and global interactive buckling of welded rectangular box-section columns

M. Radwan *, B. Kövesdi

Faculty of Civil Engineering, Department of Structural Engineering, Budapest University of Technology and Economics, Műegyetem rkp. 3, Budapest 1111, Hungary

ARTICLE INFO

Keywords:
Welded box-section
Rectangular box-section
Interactive buckling
Local buckling
Global buckling
Equivalent geometric imperfections

ABSTRACT

In recent years, the construction industry has witnessed a growing preference for welded box-sections due to their ease of fabrication and improved stability characteristics. Nonetheless, welded box-sections are prone to various instabilities, which can be classified into three categories: global buckling, local buckling, and interactive buckling. amongst these, interactive buckling is of primary concern as research in this area is still limited. Currently, there is a lack of viable options to effectively address the nonlinear interaction of global and local buckling. The equivalent imperfections provided by the Eurocode were developed based on an elastic design approach and are not suitable for geometrically and materially nonlinear analysis (GMNIA). Therefore, the applicable equivalent geometric imperfections should be revised and improved to make them suitable for plastic analysis. The authors previously investigated the interactive buckling resistance of welded square box-sections and developed suitable imperfections that can be used for GMNI analysis. However, the study was focused only on square box-sections. In the current research, the interactive buckling capacities of square and rectangular welded box-sections are investigated. A general rule for imperfection combination is proposed, which can be applied to all welded box-section columns. This makes the application of numerical model-based design more accurate for box-section columns, as well as significantly improves the general applicability of GMNI analysis-based resistance calculations.

1. Introduction

Slender columns experience pronounced global and local deformations, making them vulnerable to interactive buckling. This interaction can significantly reduce the capacity of compressed members, which could lead to premature failure of these structures. Therefore, the accurate consideration of interactive buckling is a key issue in the stability design of slender box-section columns. It is well-known from previous investigations that these sections exhibit highly unstable post-buckling paths and are, therefore, more susceptible to imperfections, leading to a lower buckling capacity than non-slender sections. Shen and Wadee demonstrated this by developing a nonlinear variational model for thin-walled hollow section struts with initial local and global imperfections. They found that in combining imperfections, an additional 10% load drop was present compared to pure local or global buckling. They also observed a transition from unstable to mildly stable post-buckling behaviour as the magnitude of imperfections is increased [1–3]. Recent studies have shown that the interaction of global and local buckling is not accurately considered in current design approaches [4, 5]. Analytical and numerical model-based design approaches should be further improved to estimate the capacity of welded box-sections accurately. The authors have previously developed combinations of equivalent global and local imperfections for welded box-section columns that accounts for the nonlinear interaction effect, however, the study was limited to square box-section columns. The current research aims to expand the scope of the previous study by proposing combinations of equivalent local and global imperfections for both square and rectangular sections highlighting the key differences between the two. The proposed imperfection combinations can be used in the FEM-based design approach.

There are two main methods that can be used in the process of designing sections against buckling. The first method uses buckling curves and takes the local and global buckling instabilities into consideration. The second method utilises numerical modelling based on GMNIA (geometrical and material nonlinear analysis with imperfections), which can accurately capture the buckling behaviour if appropriate imperfections and residual stress patterns are applied. However, modelling residual stresses poses a challenge to designers; hence, it is

* Corresponding author.
E-mail address: mohammad.radwan@emk.bme.hu (M. Radwan).

https://doi.org/10.1016/j.tws.2023.111140
Received 30 March 2023; Received in revised form 23 August 2023; Accepted 24 August 2023
Available online 28 August 2023

common to utilise equivalent geometric imperfections that account for the effects of residual stresses and geometrical imperfections, as well. A key factor in performing GMNIA-based design lies in carefully selecting the appropriate and accurate magnitudes of equivalent geometric imperfections. Therefore, the primary objective of this paper is to determine the most appropriate magnitudes of imperfections for local and global interactive behaviour.

In the current study, a numerical model is developed and validated against experimental tests conducted on square and rectangular sections available in the literature. The numerical model is employed to perform extensive parametric studies covering a wide range of local and global slenderness ratios in order to estimate the accurate resistance of welded box-section columns correctly. Finally, the determined accurate resistance is used to evaluate several combinations of equivalent local and global imperfections, and suggestions are made for imperfection combinations that can be used in the FEM-based design of welded box-section columns.

2. Literature review

2.1. Previous investigations on the local and global interaction buckling resistance

Several researchers conducted extensive investigations of the interactive buckling of steel columns. Van der Neut [6] investigated the interaction of global and local buckling behaviour of an idealised thin-walled column made of two flanges connected by an infinitely thin web. The mechanical behaviour of the interactive buckling was explained, and the relationship between the buckling load and the length of the column was demonstrated. The emphasis was placed on identifying the regions exhibiting stable and unstable behaviour depending on the slenderness of the column. Rasmussen and Hancock [7] investigated the geometric imperfections in plated structures experiencing interactive buckling, and developed an analytical technique to expand the measured geometrical imperfections based on the buckling modes. Schafer [8,9] investigated the interaction of local, distortional, and global buckling behaviour of thin-walled columns, which resulted in the improvement of the Direct Strength Method. Shen and Wadee investigated the interactive buckling of hollow section struts through local and global imperfection sensitivity studies [1], and developed a hybrid design method combining European column curves and the Direct Strength Method [10]. The study pointed out that the effective width method can be conservative in some parametric ranges [10]. Becque and Rasmussen [11] investigated the interactive buckling of stainless steel lipped channel columns and found that ultimate load and effective length curves show a slight flattening around the local buckling load in accordance with van der Neut's theory [6]. Based on a numerical study [12], it was concluded that the current design standards are conservative for stainless steel lipped channel columns for local slenderness $\bar{\lambda}_p < 1.1$, and less conservative for larger slenderness as the interaction effect becomes more pronounced. Cao et al. [13] experimentally investigated interactive buckling in H-sections and concluded that the current Eurocode [5] design rules slightly underestimate the ultimate load of welded H-section members fabricated of 800 MPa steel. Therefore, an enhanced design model was proposed, which gives more accurate buckling resistance values. Yuan et al. [14] investigated stainless steel box-sections and proposed a modified design formula, which incorporated new sets of imperfections and limiting slenderness values.

Despite the considerable research on interactive buckling, a limited number of investigations were performed on welded box-sections. Usami and Fukumoto [15,16] conducted experiments on HSS columns to study interactive buckling and developed a formula to determine the interactive buckling capacity. Chiew et al. [17] conducted 17 tests on S235 box-section steel columns and observed that the failure mode was global buckling for relatively long columns with low b/t ratios, where the global imperfection had a significant influence. Local buckling of the plates was observed besides overall buckling for high b/t ratios. Degée et al. [18] conducted an experimental and numerical study on welded rectangular sections made of S355, encompassing six samples with varying global slenderness ratios while keeping the local slenderness ratio constant. In addition, a numerical parametric analysis was conducted on rectangular box-sections. The authors recommended to apply global imperfection of $L/1000$ and local imperfection of $b/1000$ in conjunction with residual stresses in the numerical model. However, if residual stresses are not applied, they proposed using global imperfection of $L/750$ and local imperfection of $b/250$. It was found that the design method in EN1993–1–1 [5] does not accurately capture the interactive buckling of slender welded box-sections. The existing buckling curve "b" specified in EN 1993–1–1 [5] was overly conservative for welded box-section columns, and an upgraded curve "a" is proposed that more accurately reflects the experimental and numerical results. A new design method was introduced to determine the interactive slenderness of normal and high-strength steel columns. This method incorporated a new global slenderness, referred to as $\bar{\lambda}_{int}$, which accounts for the effect of local buckling. Pavlovčič et al. [19] performed eight tests on S355 welded and cold-formed slender thin-walled box-section columns subjected to concentric and eccentric compression. Based on their numerical studies, it was found that columns subjected to pure compression are highly susceptible to initial imperfections with a reduction in capacity of 45%, however, when combining different imperfections, the reduction is of a smaller magnitude compared to the effect of independent imperfections. The authors tested different combinations of equivalent geometric imperfections and found that the Eurocode recommendations for equivalent imperfections can be used for columns with thick welds. Kwon and Seo [20] investigated welded box-sections fabricated from 6.0 mm steel plates with a yield strength of 315 MPa, and proposed the direct strength method (DSM) to estimate the buckling resistance of welded box-section columns. Khan et al. [21] tested HSS slender welded box-section columns. Based on their research, medium-length samples failed by interactive buckling (combined global and local buckling) and suggested a reduction factor to take the interactive effect into consideration. In the FEM study of the test specimens, $b/1000$ and $L/1000$ were used as local and global imperfections, respectively. Heavy and light residual stress patterns were examined, as well. The study concluded that the buckling curve "b" specified in Eurocode is suitable for determining the interactive buckling of welded box-sections and that there were no major differences between heavily and lightly welded specimens. Yang et al. [22] experimented on S235 and S355 medium-length columns to study the global and local interactive buckling. In this study, a total of twelve specimens were tested, comprising ten rectangular hollow sections (RHS) and two square hollow sections (SHS), all of which exhibited failure primarily attributed to interactive buckling. It was found that the influence of the residual stresses on the buckling capacity is around 10–20% for medium-length columns, while the effect is less pronounced for significantly low- or high-slenderness columns. The authors suggested the buckling curve "a" to be used for S960 steel grade. Schillo et al. [4] examined the interactive buckling of welded box-section columns made of S500 and S960, with high b/t ratios. These columns experienced both global and local buckling at various global slenderness ratios. Using experimental and accompanying numerical investigations, the authors proposed an alternative design approach, where the effect of local buckling was introduced to the Eurocode global buckling calculation method using an equivalent local imperfection (e_p).

Radwan and Kövesdi [23] conducted a numerical investigation on square welded box-section columns to accurately estimate the interactive buckling resistance on a broad range of local and global slenderness ratios for several steel grades. The authors developed combinations of global and local imperfections with residual stresses to estimate the interactive buckling capacity accurately taking into account the

local-global interactive nonlinear behaviours. In another research [24], the authors developed equivalent local and global imperfection combinations that effectively approximate the accurate resistance, and found that the proposed imperfections meet the safety requirements specified in the Eurocode. Müller et al. [25] investigated the interactive buckling of hot-rolled and cold-formed square and rectangular hollow sections. GMNI analyses were performed to derive practical decision criteria for combining the local and global imperfections depending on the slenderness values of $\alpha_{cr,\ loc}$ and $\alpha_{cr,\ glob}$, where $\alpha_{cr} = \frac{1}{\lambda}$. A decision tree was proposed to determine the local and global imperfections based on certain slenderness limits $\alpha_{cr,\ loc} = 2.2$ and $\alpha_{cr,glob} = 25$. It was concluded that in cases where both limits are exceeded, the imperfections should be neglected. The authors suggested to use the proposed rules instead of the Eurocode rule stating that the accompanying imperfection should be reduced to 70%, as the latter would require performing the analysis twice.

To summarise, several studies investigated the interaction buckling behaviour of different types of steel columns. Depending on the studied slenderness range, some studies emphasised that the curve "b" of EN 1993–1–1 [5] often underestimates the buckling capacity, while other studies found that it is suitable for welded box-section. Various studies utilised $L/1000$ and $b/1000$ as global and local imperfections with applied residual stresses to estimate the interactive buckling resistance. Several researchers suggested applying a reduction factor accounting for the combined buckling effect, and defining a new interaction slenderness parameter to take the local buckling effect into account. The residual stresses and initial imperfections play a significant role in determining the interactive buckling capacity of columns. Accurate consideration of them can lead to a more economical design. It is possible to conclude that the interactive buckling resistance of welded box-section requires further investigations to adequately address the shortcomings of previous research programs, including using constant value imperfections to model local and global imperfections and utilising equivalent geometric imperfections that are not developed for GMNI analysis.

2.2. Previous investigations on the global and local imperfection magnitudes

2.2.1. Global imperfection

The maximum manufacturing tolerance is currently set at $L/750$, as per EN 1090–2:2008+A1:2011 [26] (now superseded by EN 1090 2:2018 [27]). However, some studies suggest that a global imperfection of $L/1000$ can be used [4,18,23,24,28], provided that residual stresses are modelled. Rondal and Maquoi [29] introduced equivalent imperfections, now utilised in the Eurocode buckling curves, representing a sinusoidal initial imperfection. EN1993–1–1 [5] and prEN1993–1–1 [30] suggest that the equivalent bow imperfection magnitudes used in GMNIA may be determined in two ways, either by calibrating the imperfection magnitudes against the buckling curves or by using approximate tabulated values. Generally, the tabulated values are more conservative compared to the calibrated values against the buckling curves.

Walport et al. [31] showed that the equivalent bow imperfections in the Eurocode are not suitable to be used in GMNI analyses, as these imperfections were developed based on elastic analyses. The authors suggested Eq. (1) to determine the imperfection magnitude (where L is the length of the member and α is the imperfection factor according to EN1993–1–1 [5]). This equivalent imperfection formula was developed based on a numerical parametric study and a calibration process. The authors calibrated the imperfection formula based on the resistance obtained from a numerical model incorporating a global imperfection of $L/1000$ and the modelling of residual stresses.

$$e_0 = \frac{\alpha L}{150} \tag{1}$$

Lindner et al. [32,33] studied equivalent imperfections for columns under pure compression, adopting an initial bow imperfection in the shape of a sin curve and considering e_0 as the maximum amplitude. The authors proposed the application of tabulated equivalent geometrical imperfections using Eq. (2), where α represents the imperfection factor, β denotes the reference relative bow imperfection, L indicates the length of the member, and ε is determined based on the strength of the material. The proposed imperfections are independent of slenderness and effective length to simplify the determination of the imperfection.

$$\frac{e_0}{L} = \frac{\alpha\beta}{\varepsilon} \tag{2}$$

Somodi et al. [34] determined equivalent global imperfections by calibrating their values against EN1993–1–1 [5] buckling curves using GMNI analysis for square and rectangular sections. The authors suggested two formulas; a slenderness-dependant accurate formula according to Eq. (3) and a simplified formula (Eq. (4)) based on statistical evaluations to provide an average level of safety for the buckling resistance calculations. This simplified approach is independent of the relative slenderness ratio and the geometry of the cross-section. The simplified formula depends on the steel yield strength of the cross-section, where $\varepsilon = \sqrt{\frac{235}{f_y}}$, and α is the imperfection factor set in EC3 [5]. In Eq. (3), $\bar{\lambda}_g$ is the global slenderness ratio according to EN1993–1–1 [5].

$$e_0 = \frac{L}{\frac{\varepsilon}{\alpha}\left(\bar{\lambda}_g^{-3.8} - 26{\cdot}\bar{\lambda}_g + 168\right)} \tag{3}$$

$$e_0 = \frac{\alpha L}{150\varepsilon} \tag{4}$$

2.2.2. Local imperfection

Using the Winter-type buckling curve [35] to calculate the local buckling resistance, has been criticised by many researchers for overestimating the buckling resistance of welded box-section columns [36–38]. As specified in Table C.2 of EN1993–1–5 [35], it is recommended to use equivalent geometrical imperfections unless a more detailed analysis of the imperfections is performed. Eurocode suggests an amplitude of at least $b/200$, where b is the shorter span. The magnitude of this imperfection was primarily calibrated to align with the Winter-type buckling curve, resulting in a local buckling capacity that closely approximates the one determined by the buckling curve. Based on experimental and numerical investigations, it was found that the buckling curves of Annex B of EN1993–1–5 [35] and Schillo et al. [36,39] provide better estimations of the local buckling resistance compared to the Winter-type curve [4,37]. Consequently, the authors conducted new calibrations [37] to determine equivalent geometric imperfections that yield the buckling resistances of the buckling curve available in Annex B of Eurocode EN1993–1–5 [35] and the buckling curve developed by Schillo et al. [36,39]. The calibrated imperfection formula is a function of the relative slenderness ratio $\bar{\lambda}_p$ and the yield strength f_y of the cross section, as shown in Eqs. 5,6. A large database was used to perform a statistical evaluation of imperfections. It was found that utilising $b/125$ as a constant value for local imperfection yields the best average estimation of the buckling resistance [40], as provided by the buckling curve developed by Schillo et al. [36,39].

$$\frac{b}{f_{0,local}} \tag{5}$$

$$f_{0,local} = \begin{cases} \frac{1}{\bar{\lambda}_p^{2.2}}{\cdot}\left(200 - 0.2{\cdot}f_y\right), & \bar{\lambda}_p \le 1.35 \\ \frac{1}{\bar{\lambda}_p}{\cdot}\left(160 - 0.2{\cdot}f_y\right), & \bar{\lambda}_p > 1.35 \end{cases} \tag{6}$$

Table 1
Applied global and local imperfections.

Imperfection Type	Residual stresses applied	Residual stresses not applied
Global Imperfection	$\frac{Member\ length\ (L)}{1000}$	Walport et al. [31] Eq. (1) ($e_0 = \frac{\alpha L}{150}$) Somodi et al. [34] Eq. (3) Somodi et al. [34] Eq. (4) $\left(e_0 = \frac{\alpha L}{150\varepsilon}\right)$
Local Imperfection	Radwan and Kövesdi [37 Calibrated imperfections to Annex B curve that depend on f_y and $\bar{\lambda}_p$ with a maximum imperfection of $\pm b/125$, according to Figure 15 of [37]	Radwan and Kövesdi [37] Eq. (5) Radwan and Kövesdi [40] ($\frac{b}{125}$)

2.3. Executed research strategy

This study aims to assess if the previously proposed imperfection combinations, originally developed for square box-sections, can be applied to rectangular ones. A comparison between the interactive buckling capacity of square and rectangular box-sections is made to show the difference in the behaviour of both sections on a wide local and global slenderness range. Several width-to-height ratios (b/h) are studied, including 1.0, 1.25, 1.5, 1.75 and 2.0, and the investigation is specifically conducted for steel grade S355. One parametric study is performed to determine the accurate buckling resistance using applied residual stresses. Three additional parametric studies are performed to find equivalent global and local imperfections that can be utilised for square and rectangular welded box-sections. Finally, two additional parametric studies are conducted to show the effect of reducing the accompanying imperfection factor when a leading imperfection is chosen as per Annex C of EN1993–1–5 [35]. Table 1 provides a summary of the imperfections utilised in this research.

This research program is summarised as follows:

1. Development and validation of the numerical model is done through a comparison with test results available in the international literature.
2. Appropriate local geometric imperfection is utilised to control the local buckling capacity based on the buckling curve specified in Annex B of EN 1993–1–5 [35]. The magnitude of the applied imperfection varies depending on f_y and $\bar{\lambda}_p$ of each analysed cross-section, as detailed in [37], with a maximum limit of $\pm b/125$, which adheres to European manufacturing tolerance, as per EN 1090–2:2018 Table B.4 No. 3 [41].
3. Global imperfection of $L/1000$ is used with applied residual stresses to control the global buckling capacity, as proposed by several researchers [18,42].
4. A numerical parametric study is performed to determine the accurate buckling resistance of square and rectangular box-section columns using the combinations of imperfections and residual stresses given in steps 2 and 3.
5. A numerical parametric study is performed with the equivalent imperfections using slenderness-dependant formulas calibrated for global and local buckling curves, according to Eq. (3) and Eq. (5), respectively.
6. A numerical parametric study is performed with the equivalent local and global imperfections previously developed for welded box-sections, according to Eq. (1) and Eq. (4) for global imperfection and a constant value of $b/125$ for local imperfection, as it was found to lead to an accurate estimation of the local buckling resistance [40].
7. To further examine the impact of different combinations of local and global geometric imperfections, supplementary numerical parametric analysis is conducted in accordance with the design guidelines outlined in EN 1993–1–5 [35], where the leading imperfection is chosen, and the accompanying imperfection is reduced to 70%.
8. Reliability assessment is performed to ensure the applicability of the proposed imperfection combinations for square and rectangular box sections.

3. Development and validation of the numerical model

3.1. The developed numerical model

A numerical model is developed using the Ansys finite element software [43] to determine the interactive buckling capacity of square and rectangular welded box-section columns. A four-node full thin shell element model is developed, as shown in Fig. 1.*a*. Geometrical and material nonlinear analysis with imperfections (GMNIA) is employed to calculate the buckling resistance using the full Newton-Raphson solver technique. The convergence was checked based on the norm Euclidean of the unbalanced internal forces. The convergence tolerance factor was 0.1%. Half sin-wave imperfections are used to model the global and local imperfections. The width of the wider plate is denoted by (b), while the width of the shorter plate is denoted by (h), as shown in Fig. 1.*b*. The applied local imperfections are based on hand-defined method, where the number of half sin-waves, which are used for local buckling, is determined by dividing the plate length (L) by the plate width (b) and rounding to the nearest integer [19]. The same number of half sin-waves is applied to all the sides of the column, with adjacent sides having opposite amplitudes. The configuration is illustrated in Fig. 1.*a*, where outward imperfections are considered positive. This is a simplified approach to model the local imperfection, which leads to a reliable estimation of the buckling resistance. The global imperfection is defined as a half sin-wave spanning the entire length of the column. The half sin-wave is applied along the x-axis, as shown in Fig. 1.*a*. The columns are designed to fail by buckling on the minor axis (x-axis). Both global and local imperfections were applied simultaneously to study their interactions, as depicted in Fig. 1.*a*. Boundary conditions and loads are applied to master nodes created at the geometrical centre of the column.

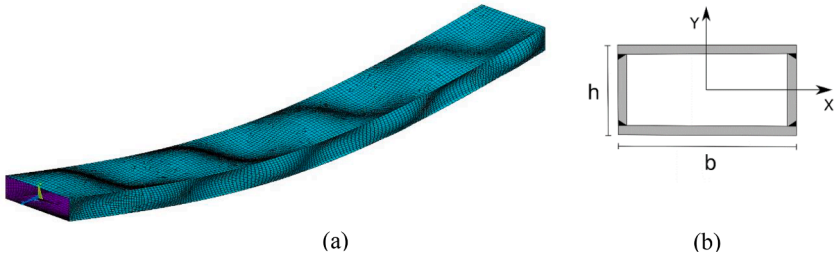

(a) (b)

Fig. 1. a) the developed numerical model and b) the general cross-section.

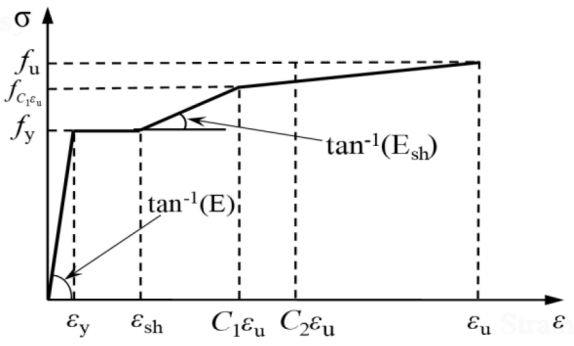

Fig. 2. Material model according to prEN 1993–1–14 [44,45].

All 6 DOFs are coupled between the nodes of the end cross sections and the master nodes. The first master node is restrained in the global direction in UX, UY, UZ and RZ, and the second master node is restrained in UX, UY and RZ, where U and R indicate restraining translation and rotation, respectively. The material model shown in Fig. 2 is utilised to simulate the behaviour of normal strength steel (NSS), which is a quad-linear material model developed for hot-rolled steel. This material model accurately captures the strain-hardening behaviour of NSS, and it was developed based on a large number of coupon tests by Yun and Gardner [44].

This study employs a multilinear inelastic material model that defines the stress-strain relationship using a set of coefficients. Table 2 lists the required coefficients for the model, including the yield strain $\varepsilon_y = f_y/E$, strain hardening strain ε_{sh}, and modulus E_{sh}. Here, $A = 0.2$ is the elongation after fracture, C_1 is the "cut-off" strain coefficient, and C_2 is used to determine the slope of strain hardening E_{sh}. In this research program, a modulus of elasticity of $E = 210{,}000$ MPa and a Poisson's ratio $\nu = 0.3$ are used for all numerical tests.

Several researchers highlighted the significance of the residual stresses model [46,47], as they could lead to premature failure and loss of stiffness under compression. The details of the residual stress model, according to the ECCS recommendations, are illustrated in a previous research study by the authors [37].

3.2. Validation of the numerical model

To efficiently conduct extensive parametric studies, it is important to select a mesh size that leads to accurate resistance while also being numerically feasible. Therefore, a mesh sensitivity analysis for the smallest and largest plate widths in the study was performed beforehand. The analysis revealed that a mesh consisting of 16 elements along the plate width provides an accurate estimation of the buckling capacity, with an error of less than 1%, as shown in the previous research work [24]. Four distinct research programs are employed to validate the model, with several samples taken from each research program with various b/h ratios ranging from 1.0 to 1.96. The measured values of the studied columns are incorporated into the numerical model according to the specified research programs. To ensure consistency with previous research, a global imperfection of $L/1000$ and the calibrated local geometrical imperfections and residual stress, as presented in *Fig.15* of the prior research [37], are applied to the numerical model. The samples utilised for the validation process are presented in Table 3, where f_{local_h} and f_{local_b} are the imperfection scaling factors applied as (h/f_{local_h}) or (b/f_{local_b}). The full sample set has a mean and CoV of 0.998 and 0.069, respectively. Most of the samples demonstrate a high level of agreement with the numerical model, showing a difference of maximum 5%, as shown in Table 3. Larger discrepancies may be attributed to unintended eccentricities in the experimental tests. To compare the numerical and experimental results, two samples are presented in Fig. 3. The arc-length method is used to trace the loading path until the failure point is reached. The left-hand side figure depicts a test sample from the research program conducted by Yang et al. [22], while the sample in the right-hand figure is taken from a research program conducted by Pavlovčič et al. [19]. Both samples exhibit similar behaviours and buckling capacities as observed in the experimental tests. This shows the

Table 2
The applied material model parameters.

	f_y [MPa]	f_u [MPa]	ε_{sh} [-]	ε_u [-]	$C1$ [-]	$C2$ [-]	E_{sh} [MPa]	$C1 \cdot \varepsilon_u$ [-]	$f_{C1\varepsilon u}$ [MPa]
S355	355	510	0.015	0.182	0.31	0.448	2310	0.057	451

Table 3
The results of the validation process.

b/h	λ_g	λ_{p_b}	λ_{p_h}	b (mm)	h (mm)	t (mm)	L (mm)	f_y (MPa)	f_u (MPa)	Local imp. $f_{local\text{-}b}$	Local imp. $f_{local\text{-}h}$	$F_{u,exp}$ (kN)	$F_{u,num}$ (kN)	$\frac{F_{u,num}}{F_{u,exp}}$
Chiew et al. [17]														
1	0.37	0.71	0.71	80	80	2	1100	261	360	2130	2130	159	150.75	0.95
1	0.47	0.71	0.71	80	80	2	1500	261	360	2130	2130	140	141.69	1.02
1	0.59	0.71	0.71	80	80	2	1850	261	360	2130	2130	143	134.51	0.94
1	0.50	0.71	0.71	80	80	1.4	1850	261	360	566	566	72	72.31	1.01
Yang et al. [22]														
1.88	0.44	0.94	0.50	254	135	5.5	2251.6	309	458	496	2200	1057.7	1081.55	1.02
1.96	0.67	1.12	0.57	309	158	5.6	4159.9	309	458	556	2200	1176.9	1162.25	0.99
1.92	0.40	1.50	0.78	404.5	210	5.4	3585.3	309	458	125	2040	1284.6	1261.58	0.98
1.96	0.38	1.82	0.93	491.2	251.4	5.4	4378.1	309	458	125	497	1287.6	1352.61	1.05
1.94	0.48	1.24	0.64	312.5	161.8	5.69	2786.9	385	545	359	2200	1414.6	1430.83	1.01
1.93	0.44	1.56	0.81	312.1	163	6.05	4165.6	385	545	125	1300	1456.7	1619.3	1.11
Pavlovčič et al. [19]														
1.25	0.79	1.11	0.89	200	160	4	4000	373.4	452	548	570	706	711.6	1.01
1.25	1.03	1.11	0.89	200	160	4	5200	373.4	452	548	570	564	623.66	1.11
Kwon [48]														
1.36	0.62	1.02	0.75	300	220	6	5000	315	490	480	2200	1676.1	1471.41	0.88
1.55	0.67	1.05	0.68	310	220	6	5000	315	490	493	2200	1627.3	1414.2	0.87
1.07	0.46	1.05	0.99	310	290	6	5000	315	490	493	483	1524.4	1554.6	1.02
													Mean	0.998
													COV	0.069

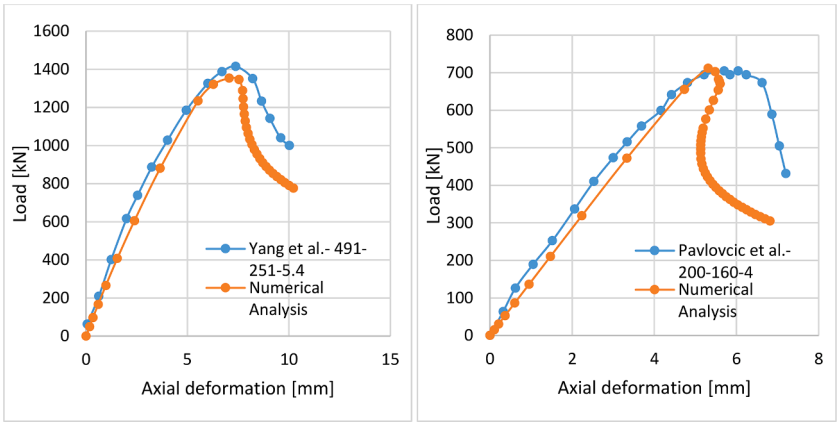

Fig. 3. The load-deformation diagram of the experiment and the numerical analysis: a) Yang et al. 491–251–5.4 [22] and b) Pavlovčič et al. test specimen 200–160–4 [19].

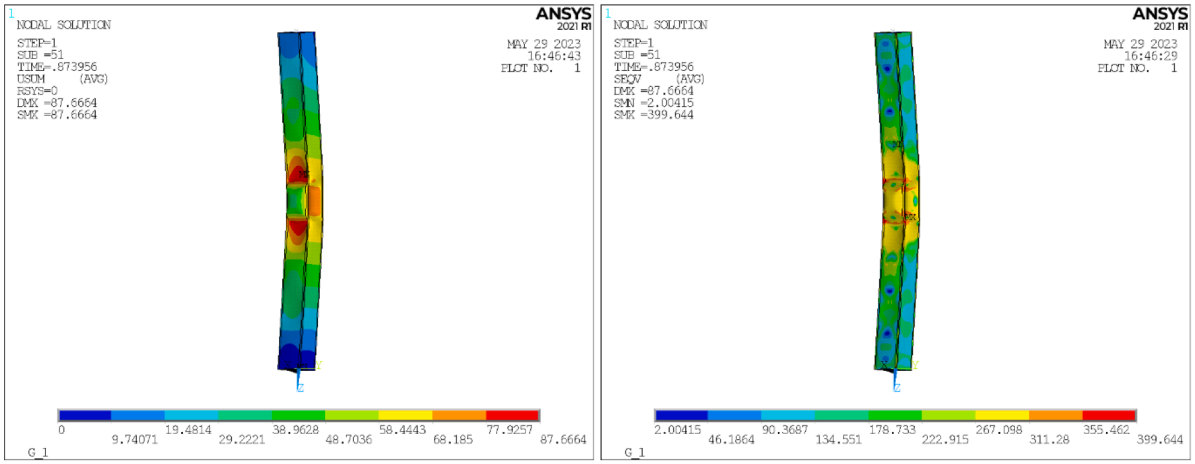

Fig. 4. The failure mode at the final load step of Yang et al. test specimen 491–251–5.4 [22]; a) deformed shape, b) Von-Mises stresses.

ability of the model to capture the interactive buckling under investigation. Fig. 4 shows the interactive buckling mode of a sample from a research study by Yang et al. [22], where $b = 491$ mm, $h = 251$ mm, and $t = 5.4$ mm. The figure also shows the deformations and the Von-Mises stress of the sample. It can be seen that the column failed due to minor axis buckling, particularly in the wider plate of the column, as it has a larger local slenderness compared to the shorter plate. The validation process proves the accuracy and reliability of the proposed method for estimating the interactive buckling resistance.

3.3. Geometrical properties of the sections used in the study

In this study, the analysed sections have h/t and b/t ratios larger than 40 with global slenderness ratio ($\bar{\lambda}_g$) larger than 0.2 and local slenderness ratio ($\bar{\lambda}_p$) larger than 0.7 for both the width and the height of the cross-section. Table 4 provides an overview of the geometric properties of all the samples in this study. Five different b/h ratios are studied to investigate the effect of b/h ratios on the interactive buckling resistance of the welded box-sections. The plate width (b) is determined by multiplying the plate height (h) by the b/h ratio.

Table 4
Geometries of the studied cross-sections.

Property [unit]	Range
Global slenderness ratio $\bar{\lambda}_g$ [-]	0.2–2.0
Local slenderness ratio $\bar{\lambda}_{p-h}$ [-]	0.9–2.0
Plate thickness t [mm]	3–6
Plate height h [mm]	250
Plate width b [mm]	250 - 500
Plate length L [mm]	750–17,500
Steel yield strength f_y [MPa]	355
b/h ratios [-]	1, 1.25, 1.5, 1.75, 2.0

4. Results of the parametric studies

4.1. Geometrical imperfections with applied residual stresses

A numerical parametric study is executed to determine the accurate resistance of square and rectangular columns by performing the analysis with the combinations of imperfections and residual stresses developed in previous research works [23,37]. A combination of $L/1000$ as global imperfections, local imperfections calibrated to the Annex B curve of EN1993–1–5 [35] with a maximum value of $b/125$ as per EN 1090–2:2018 Table B.4 No. 3 [41], and residual stresses [37] is used. The applied local imperfection for each plate of the column depends on its local slenderness ratio $\bar{\lambda}_p$. As was shown in previous research [37], a

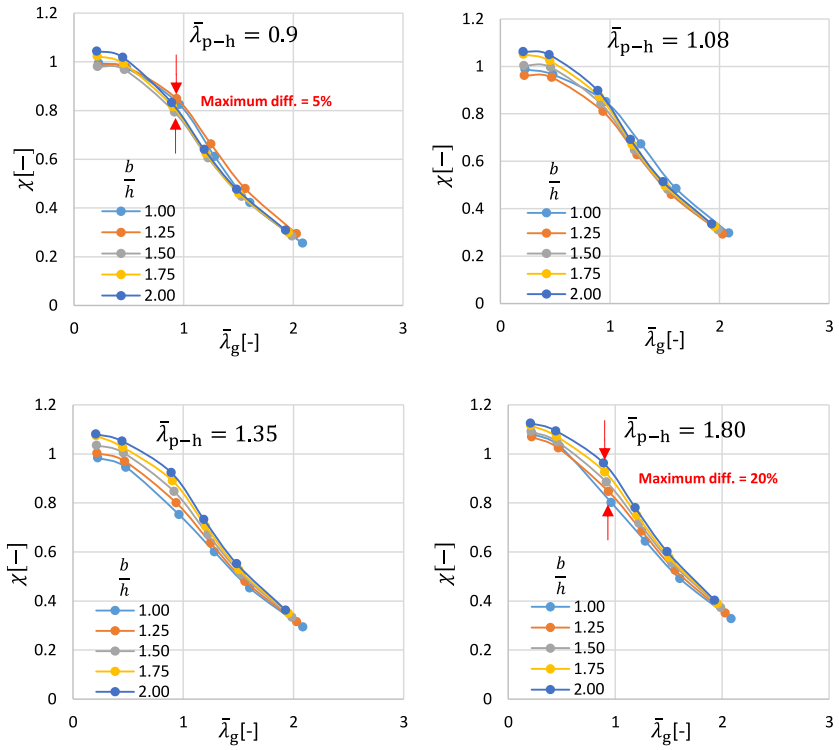

Fig. 5. Relationship between the global slenderness ratio $\bar{\lambda}_g$ and global reduction factor χ curves for various local slenderness ratios $\bar{\lambda}_{p-h}$ and b/h ratios.

higher local slenderness ratio $\bar{\lambda}_p$ requires a larger imperfection to be applied in the numerical model to yield the resistance of the buckling curve. Fig. 5 shows the result of the parametric study, where the x-axis shows the global buckling slenderness ratio $\bar{\lambda}_g$ and the y-axis shows the reduction factor χ for studied $\bar{\lambda}_{p-h}$ including 0.9, 1.08, 1.35 and 1.8. The reduction factor is determined as follows $\chi = \frac{N_{analysis}}{A_{eff} \cdot f_y}$, where $N_{analysis}$ is the buckling resistance obtained using the numerical analysis and A_{eff} is the effective area determined using the Annex B curve.

Several b/h ratios are studied, specifically 1.0, 1.25, 1.5, 1.75, and 2.0. The differences in the reduction factor χ between the different b/h ratios are relatively small, especially for the local slenderness range $\bar{\lambda}_{p-h} < 1.1$ with a maximum difference of 5%. For $\bar{\lambda}_{p-h} > 1.1$, the difference is larger and can reach up to 20% for a very large local slenderness range $\bar{\lambda}_{p-h} = 1.8$. It can be clearly seen that the square box-section with $b/h = 1$ can be considered the lower bound for sections with larger b/h ratios. This is due to the fact that in rectangular sections, smaller plates (h) provide larger stiffness to wider plates (b), increasing the edge restraint [49] and allowing larger buckling resistances.

4.2. Equivalent geometrical imperfection

Three parametric studies are performed to determine suitable equivalent imperfection combinations that can be used in FEM-based design approaches. The applied imperfections are chosen to be independent of the slenderness ratios to provide a convenient way of applying them. As shown in the literature review, several suggestions are available for imperfections that were developed for GMNI analyses and are independent of the slenderness ratio $\bar{\lambda}_g$; the suggestions of Walport et al. [31] (Eq. (1)) and Somodi et al. [34] (Eq. (4)) are used for equivalent global imperfections in the current study. The two suggestions are highly similar; both depend on the length of the member and the α imperfection factor specified in the Eurocode. The main difference between the two is that the suggestion of Somodi et al. [34] uses ε to account for the yield strength of the steel, as this suggestion was based on the Eurocode buckling curves, while the suggestion of Walport et al. [31] was based on benchmark GMNI analyses. Both imperfections meet the safety requirements of the Eurocode based on reliability assessment studies. As for local imperfections, the authors have previously performed a comprehensive reliability assessment study to find imperfection factors that satisfy the safety requirements of Eurocode and yield accurate buckling resistances [40]. It was found that an imperfection of $b/125$ satisfies the requirements of the Eurocode, and yields reliable results to the buckling curve developed by Schillo et al. [4]. This buckling curve was found to provide an accurate estimation of the local buckling capacity of welded box-sections by conducting numerical and experimental tests. It should be mentioned that both the Annex B curve [35] and the buckling curve of Schillo et al. [4] are quite similar, showing a small difference in the estimated capacity for large local slenderness ratios $\bar{\lambda}_p$. Therefore, the imperfection $b/125$ is chosen to be used as a local imperfection factor. It is worth noting that the accurate imperfection magnitude should ideally be dependant on the slenderness. Consequently, employing an imperfection factor with a constant value yields safe resistances for the small slenderness range and slightly unsafe results for very slender structures. To demonstrate this, an additional parametric study is performed with slenderness-dependant imperfections. Table 5 summarises the studied imperfection combinations in this section.

The first parametric study is performed with slenderness-dependant imperfections, where the global imperfection is applied according to Eq. (3), and the local imperfection is applied according to Eq. (5), here

Table 5
Studied combinations of imperfections.

Combination Name	Global imperfection	Local imperfection
Slenderness-dependant combination	Somodi et al. [34], Eq. (3)	Radwan and Kövesdi [37], Eq. (5)
Walport et al. [31] combination	Walport et al. [31], Eq. (1)	$b/125$
Somodi et al. [34] combination	Somodi et al. [34], Eq. (4)	$b/125$

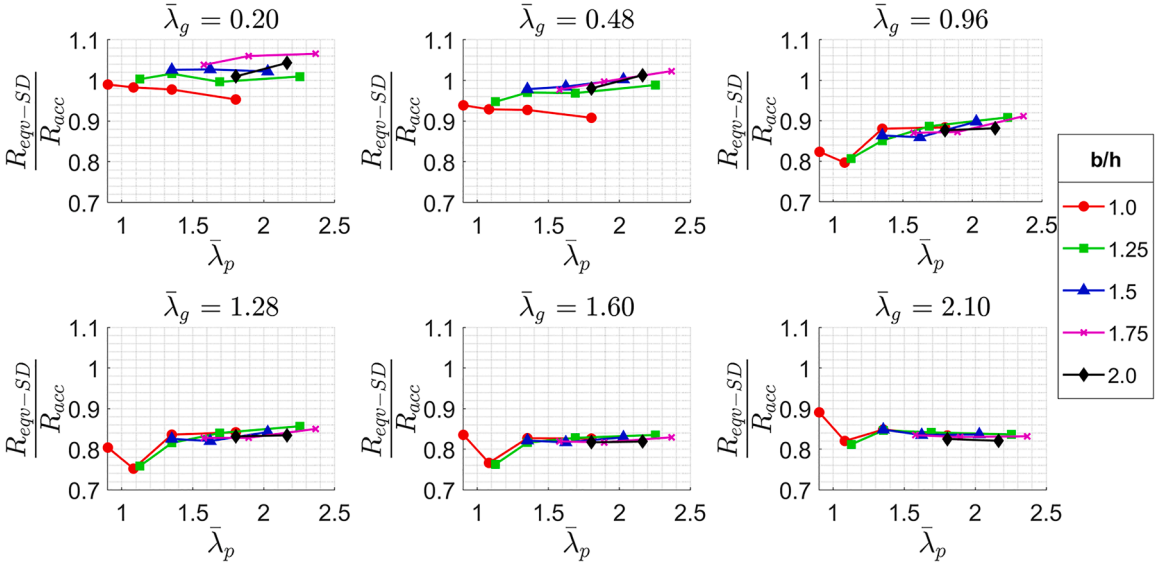

Fig. 6. Comparing the equivalent resistance ($\mathbf{R_{eqv-SD}}$) to the accurate resistance ($\mathbf{R_{acc}}$) using the slenderness-dependant combination.

Table 6
Statistical measures of the equivalent resistance to the accurate resistance using the slenderness-dependant combination.

b/h	Samples number	Mean μ	Standard deviation σ	COV	Max	Min
1	30	0.883	0.068	0.077	0.999	0.752
1.25	30	0.883	0.082	0.093	1.016	0.759
1.5	30	0.897	0.083	0.093	1.027	0.817
1.75	30	0.905	0.094	0.103	1.065	0.817
2	30	0.896	0.089	0.099	1.043	0.817
All	150	0.891	0.080	0.090	1.065	0.752

called slenderness-dependant combination. This combination is studied to highlight the dependency of applied imperfections on both local and global slenderness, and by using the slenderness-dependant imperfections, a safer resistance can be achieved. Both imperfections are applied with a 100% magnitude without any reduction. The parametric study is conducted for the same geometries described in Table 4, with a limited slenderness of 2.0, as the formulas were calibrated up to that range. The resistance obtained using the equivalent imperfection combinations will be referred to as "equivalent resistance (R_{eqv})", while the resistance obtained using the imperfection combination with residual stresses will be referred to as "accurate resistance (R_{acc})" from now on. Fig. 6 presents the results of the parametric study, illustrating six plots corresponding to the studied global slenderness ratios ($\bar{\lambda}_g = 0.2 - 2.1$). Each plot shows the relationship between the local slenderness ratio of the longer plate $\bar{\lambda}_{p-b}$ on the x-axis and the ratio of equivalent resistance (R_{eqv-SD}) to accurate resistance (R_{acc}) on the y-axis. The *b/h* ratios examined in the study are shown on each plot. Based on the individual plots in Fig. 6, it is possible to see the relationship and the differences between the analysed cross-section geometries and the trend in terms of the *b/h* ratio. It can be observed that this combination provides a safe estimation of the accurate resistance with a mean value of 0.891 and a standard deviation of 0.08 for equivalent to accurate resistance ratios. This combination usually underestimates the buckling resistance of welded box-section columns, which is expected when using equivalent geometric imperfections. It should be highlighted that the imperfection formulas for pure global and local buckling were developed independently based on

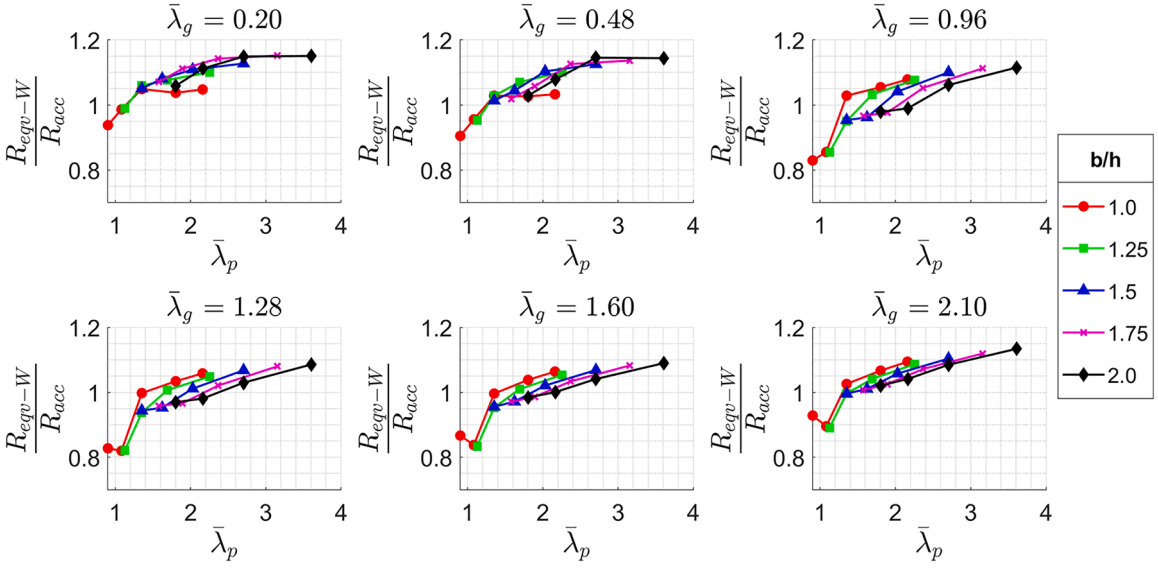

Fig. 7. Comparing the equivalent resistance ($\mathbf{R_{eqv-W}}$) to the accurate resistance ($\mathbf{R_{acc}}$) using Walport et al. [31] combination.

Table 7
Statistical measures of the equivalent resistance to the accurate resistance using Walport et al. [31] combination.

b/h	Samples number	Mean μ	Standard deviation σ	COV	Max	Min
1	30	0.960	0.085	0.088	1.067	0.820
1.25	30	0.999	0.084	0.084	1.101	0.821
1.5	30	1.036	0.060	0.057	1.127	0.944
1.75	30	1.052	0.063	0.059	1.152	0.958
2	30	1.061	0.060	0.057	1.151	0.969
All	150	1.022	0.079	0.078	1.152	0.820

calibrations of the Eurocode [5] and Schillo et al. [4] buckling curves, respectively. These curves include reductions accounting for the effect of residual stresses and imperfections; therefore, applying both imperfections with a 100% magnitude might lead to duplicating the included residual stresses.

The results shown in Fig. 6 also prove that the buckling resistances corresponding to square box-section ($b/h = 1$) are the closest to the accurate solution, as the equivalent geometrical imperfections were developed for $b/h = 1$. The results also indicate that for larger b/h ratios, the application of the equivalent geometric imperfections leads to a safe solution, which means that the equivalent geometric imperfections developed for square box-section columns can be safely used for rectangular section columns, as well. As the difference between the estimated capacities for the square and rectangular section is minimal, it is possible to apply the previously developed equivalent imperfections for rectangular cross-sections. Table 6 shows the statistical evaluation of the ratio of equivalent to accurate resistance using the slenderness-dependant combination.

The second parametric study is executed using the imperfection value proposed by Walport et al. [31] depicted in Eq. (1) as global imperfection and $b/125$ for the local imperfection referred to as Walport et al. [31] combination. The parametric study is done for the same geometries described in Table 4. The results of the parametric study are shown in Fig. 7, where R_{eqv-W} is the equivalent resistance using Walport et al. [31] combination. Two important findings can be seen in Fig. 7: (i) the buckling resistance for the $b/h = 1$ case also represents the upper-bound surface; as the b/h ratio increases, the ratio of the equivalent to accurate resistances decreases; (ii) as the local slenderness ratio increases, the ratio of the equivalent to accurate resistances increases, as well. It can be seen that as the local slenderness increases, the overestimation of the buckling resistance also increases and can reach up to 15% for very large slenderness $\bar{\lambda}_{p-b} > 2$. This comes from the fact that a constant value for local imperfection ($b/125$) is applied, which gives slightly unsafe resistances within the very large slenderness range ($\bar{\lambda}_{p-b} > 2$, which rarely occurs in the design practice). If a larger imperfection is used, the overestimation is lower, as shown in Fig. 6, with a maximum value of less than 5%. A similar trend cannot be observed depending on the global slenderness ratio; thus, the same parameter range is analysed within the entire parametric study. Upon evaluating the results in terms of the global slenderness ratio, it can be observed that when the b/h ratio is increased, there is a noticeable decrease in the ratio of equivalent to accurate buckling resistance, especially for $\bar{\lambda}_g > 0.48$. This means that the largest overestimation occurs in square sections ($b/h = 1$), and the equivalent geometric imperfection developed for them can also be applied for rectangular section columns, resulting in safer resistances. A statistical assessment is also performed on the equivalent-to-accurate resistance ratio for all the b/h ratios. The results are summarised in Table 7. A total number of 150 samples are studied, with 30 samples for each b/h ratio. It can be seen that the overall mean of all the samples equals 1.022, with a standard deviation of 0.079, indicating an excellent fit to the accurate resistance. The maximum and minimum values are 1.152 and 0.820, respectively.

The third parametric study is done by using the imperfection proposed by Somodi et al. [34] depicted in Eq. (4), referred to as Somodi et al. [34] combination. The results of the parametric study are summarised in Fig. 8, where R_{eqv-S} is the equivalent resistance using Somodi et al. [34] combination. In Fig. 8, a similar behaviour to the Walport et al. [31] combination can be observed, where the largest overestimation occurs in the region of very large local slenderness ($\bar{\lambda}_p > 2$).

Table 8
Statistical measures of the equivalent resistance to the accurate resistance using Somodi et al. [34] combination.

b/h	Samples number	Mean μ	Standard deviation σ	COV	Max	Min
1	30	0.935	0.087	0.093	1.046	0.788
1.25	30	0.973	0.088	0.090	1.093	0.790
1.5	30	1.011	0.067	0.066	1.122	0.908
1.75	30	1.026	0.070	0.068	1.146	0.921
2	30	1.035	0.067	0.065	1.144	0.934
All	150	0.996	0.084	0.084	1.146	0.788

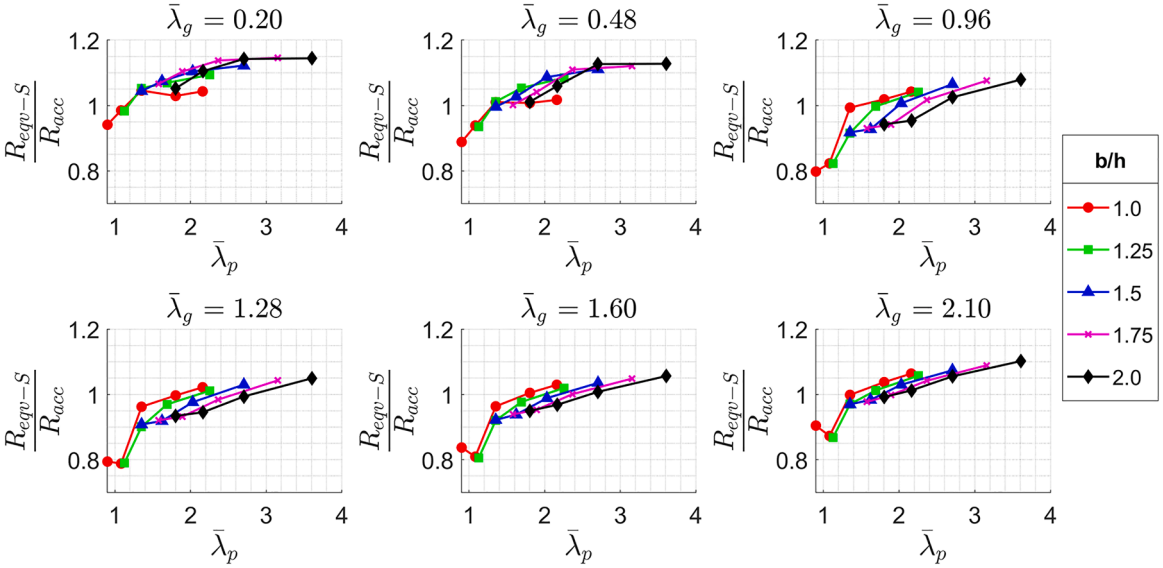

Fig. 8. Comparing the equivalent resistance ($\mathbf{R_{eqv-S}}$) to the accurate resistance ($\mathbf{R_{acc}}$) using Somodi et al. [34] combination.

Table 8 summarises the statistical evaluation of the parametric study. Applying Somodi et al. [34] combination in the numerical model leads to a safer mean value of 0.996 with a standard deviation of 0.084 and a maximum and minimum value of 1.146 and 0.788, respectively. This combination leads to smaller resistances compared to the combination that uses the imperfection proposed by Walport et al. [31]. This is due to the fact that the imperfection proposed by Somodi et al. [34] was calibrated to the Eurocode buckling curves. Therefore, when this imperfection is utilised in a more accurate GMNIA-based combination, it results in a larger scatter compared to the imperfection of Walport et al. [31], which is based on GMNI calculations.

Based on the parametric studies performed, it can be concluded that the proposed imperfection combinations can be safely used for rectangular box-section columns, as well, using the global imperfections proposed by Walport et al. [31] and Somodi et al. [34].

4.3. Reduced equivalent imperfections

The Annex C of EN1993–1–5 [35] states that in combining imperfections, a leading imperfection should be chosen, and the magnitude of the accompanying imperfection can be reduced to 70%. In this research, two parametric studies are performed to investigate the importance, effect, and accuracy of the rules for combinations of imperfections. The same geometries will be studied here, as shown in Table 4. The combinations of imperfections in Table 5 are investigated twice; (i) by choosing a leading global imperfection applied with a 100% magnitude and reducing the accompanying local imperfection to 70%, referred to as reduced local combination; (ii) by choosing a leading local imperfection applied with a 100% magnitude and reducing the accompanying global imperfection to 70%, referred to as reduced global combination. The results of the parametric studies are compared to the non-reduced combination (100% for both local and global imperfections) in Table 5 and to the accurate resistance described in the previous sections.

The slenderness-dependant combination is studied, where the global imperfection (Eq. (3)) is applied with a 100% magnitude, and the local imperfection (Eq. (5)) is reduced to 70% referred to as reduced local combination. A statistical assessment is performed on the ratio of the resistance achieved by applying the reduced local combination to the accurate resistance. Here, only the final outcomes are summarised. The reduced local combination yields resistances that are closer to the accurate buckling resistance on average, with a mean value of 0.954 and a standard deviation of 0.084. The maximum and minimum values are 1.08 and 0.883, respectively. However, the results also show that this combination yields unsafe resistances for specific slenderness ranges ($\bar{\lambda}_g$ *and* $\bar{\lambda}_p > 1.8$) with a maximum overestimation of 8%. Another parametric study is performed using a reduced global imperfection (Eq. (3)) at a magnitude of 70%, and the local imperfection (Eq. (5)) is applied with a 100% magnitude, referred to as reduced global combination. A similar statistical assessment is performed to evaluate the equivalent-to-accurate resistance ratio using the reduced global combination. The mean and the standard deviation of this combination are equal to 0.938 and 0.066, respectively. The mean value obtained for this combination is smaller compared to that of the reduced local combination. This combination provides better estimation of the accurate resistance compared to the non-reduced combination, as indicated by all mean values being below 1.0 and a maximum overestimation of 6%. It is observed that this combination provides a larger resistance compared to the non-reduced combination by approximately 7%. The largest difference occurs in the large global slenderness range, irrespective of the local slenderness ratio. Fig. 9 and Table 9 show the statistical measures of the minimum of the studied combinations. The obtained resistance using reduced global or reduced local slenderness-dependant combinations are shown in Fig. 9 as $R_{\mathrm{eqv-SDRG}}$ and $R_{\mathrm{eqv-SDRL}}$, respectively. The mean value for all the *b/h* ratios equals 0.922 with a standard deviation of 0.05. The maximum and minimum values are 1.067 and 0.911, respectively.

Table 9
Statistical measures of the minimum ratio of the studied combinations (reduced local or reduced global slenderness-dependant combination) to the accurate resistance.

b/h	Samples number	Mean μ	Standard deviation σ	COV	Max	Min
1	30	0.906	0.051	0.057	0.992	0.796
1.25	30	0.919	0.068	0.074	1.018	0.797
1.5	30	0.932	0.066	0.071	1.029	0.866
1.75	30	0.938	0.077	0.082	1.067	0.867
2	30	0.928	0.073	0.078	1.042	0.862
All	150	0.922	0.050	0.055	1.067	0.911

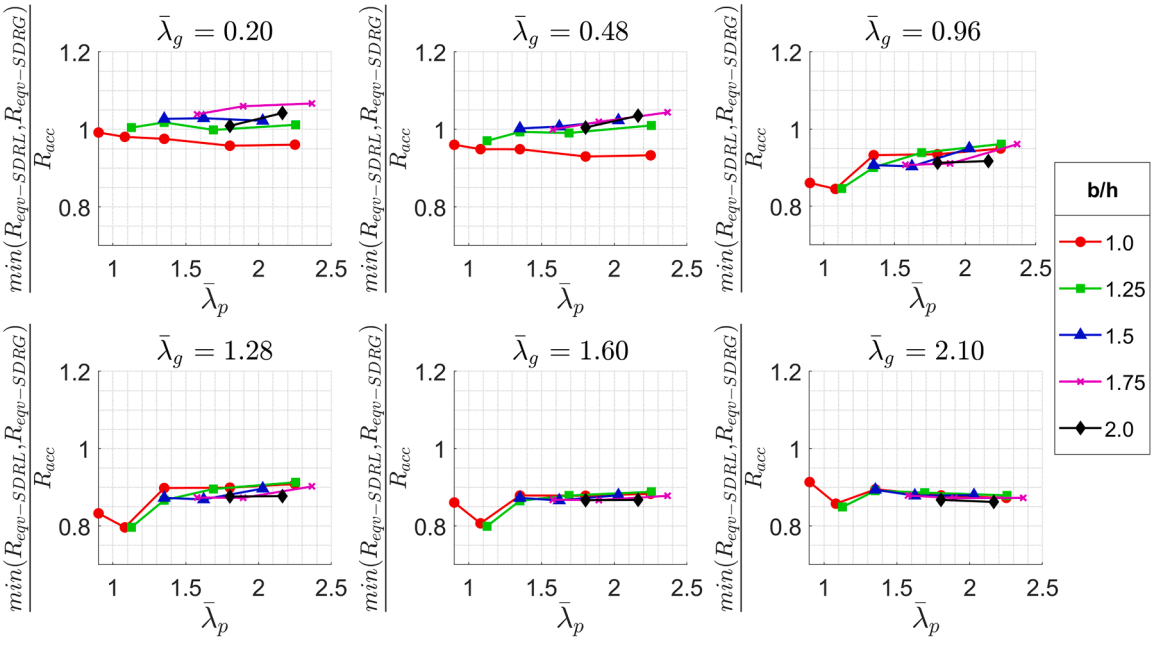

Fig. 9. The minimum ratio of the resistance of the studied combination (reduced local or reduced global slenderness-dependant combination ($\mathbf{R_{eqv-SDRL}}$, $\mathbf{R_{eqv-SDRG}}$)) to the accurate resistance ($\mathbf{R_{acc}}$).

By taking the minimum of the two imperfection combinations, a smaller mean value and standard deviation are achieved compared to combinations with a 100% magnitude. The results further indicate that there is only a small difference in the buckling resistance when comparing the application of 100% magnitudes for global and local imperfections versus reducing one to 70%; however, the computational time is doubled by investigating two different imperfection combinations. Therefore, it is recommended to apply both imperfections with a magnitude of 100%.

Somodi et al. [34] combination is studied next, where the global imperfection is determined according to Eq. (4), and the local imperfection is equal to a constant value of $b/125$. The previously discussed combinations, namely reduced global and reduced local combinations, are studied here, as well. A statistical assessment is performed on the ratio of the equivalent-to-accurate buckling resistance. Here, only the final outcomes are discussed. It is found that reducing the local imperfection results in a larger buckling resistance with an approximate increase of 6% in the region of low local slenderness ($\bar{\lambda}_{p-b} < 1.0$). The mean of all the samples is equal to 1.036 with a standard deviation of 0.077, compared to 0.996 and 0.084 for the non-reduced combination in Table 8. This represents an increase of approximately 4% based on the mean values. The accurate resistance is overestimated by 5–16% if this reduction is applied. The mean values for all the samples categorised by b/h ratios are larger than 1.0, except for $b/h<1$. It is possible to conclude that reducing the local imperfection to 70% reduces the safe range where this combination can be applied.

If the local imperfection is reduced to 70% and Walport et al. [31] global imperfection (Eq. (1)) is used instead of Somodi et al. [34] imperfection (Eq. (4)), the mean value and the standard deviation are equal to 1.062 and 0.073, respectively. The minimum and maximum values are 0.862 and 1.169, respectively. A similar parametric study is performed by employing a reduced global imperfection based on Somodi et al. [34] (Eq. (4)) at a magnitude of 70% and a local imperfection of $b/125$ at a magnitude of 100%, referred to as Somodi et al. [34] reduced global combination. It is observed that the overestimation of the non-reduced resistance is approximately 6%. The largest overestimation occurs in the region of high global slenderness range ($\bar{\lambda}_g > 1.5$), highlighting the influence of global slenderness within this specific slenderness range. The overestimation is observed across the entire local slenderness range, suggesting that it is independent of the local slenderness for all b/h ratios. A statistical assessment was conducted to evaluate the ratio of the equivalent-to-accurate resistance. The mean value for all the samples being studied is equal to 1.049 with a standard deviation of 0.077. This can be compared to the values of 1.036 and 0.077 if the local imperfection is reduced. Similarly, the mean values for all the samples categorised by b/h ratios are larger than 1.0, except for $b/h<1$. The utilisation of this combination results in overestimated resistances with an approximate range of 5–16% higher than the accurate resistance. For reduced global imperfection using Walport et al. [31] combination, the mean value and the standard deviation are equal to 1.069 and 0.076, respectively. The minimum and the maximum of the ratio are equal to 0.868 and 1.182, respectively. Fig. 10 shows the minimum of ratios of the equivalent resistances obtained using Somodi et al. [34] reduced global and Somodi et al. [34] reduced local combinations to the accurate resistance. The resistances of reduced global and reduced local combinations are shown in Fig. 10 as $R_{\mathrm{eqv-SRG}}$ and $R_{\mathrm{eqv-SRL}}$, respectively. Table 10 shows the statistical measures based on the minimum ratios of the combinations to the accurate resistance. The mean of all the samples is determined to be 1.033 with a standard deviation of 0.077. Although the mean value of the minimum of the combinations is smaller than the mean of the reduced combinations, it is still larger than the mean achieved by applying both imperfections with a 100% magnitude. However, the standard deviation of the minimum is smaller than the standard deviation of the non-reduced Somodi et al.

Table 10
Statistical measures of the minimum ratio of the studied combinations (reduced local or reduced global Somodi et al. [34] combination) to the accurate resistance.

b/h	Samples number	Mean μ	Standard deviation σ	COV	Max	Min
1	30	0.986	0.084	0.086	1.103	0.830
1.25	30	1.023	0.083	0.081	1.125	0.828
1.5	30	1.053	0.062	0.059	1.143	0.946
1.75	30	1.061	0.068	0.064	1.161	0.946
2	30	1.056	0.063	0.060	1.153	0.961
All	150	1.033	0.077	0.074	1.161	0.828

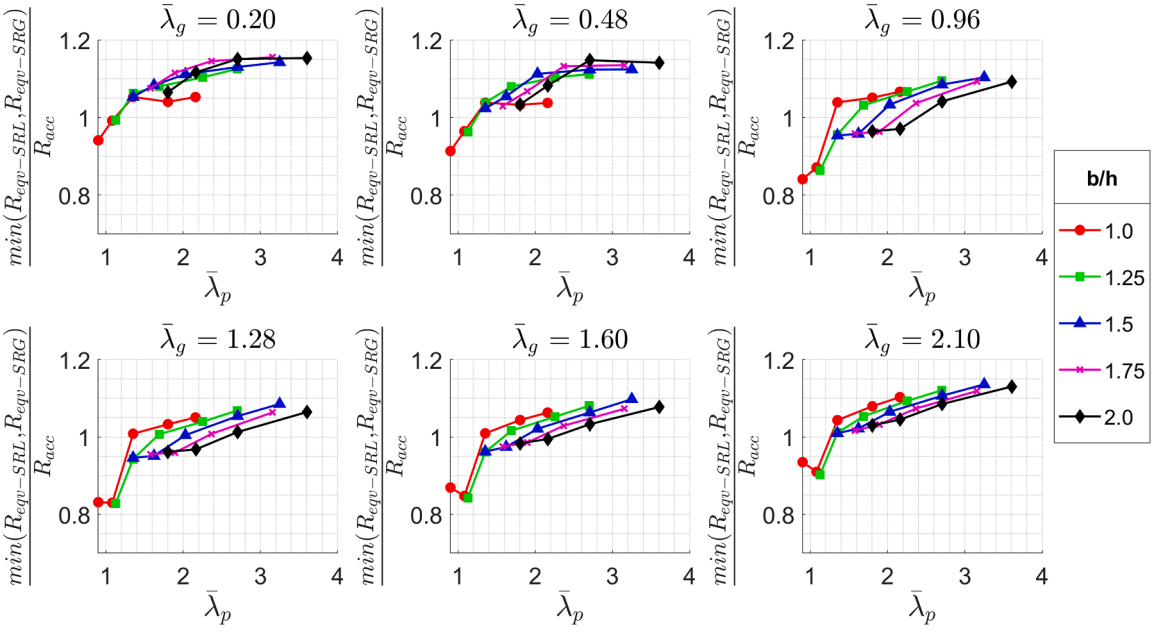

Fig. 10. The minimum ratio of the resistance of the studied combinations (reduced local or reduced global Somodi et al. [34] combination ($\mathbf{R_{eqv-SRL}}$, $\mathbf{R_{eqv-SRG}}$)) to the accurate resistance ($\mathbf{R_{acc}}$).

Table 11
Statistical measures of the minimum ratio of the studied combinations (reduced local or reduced global Walport et al. [31] combination) to the accurate resistance.

b/h	Samples number	Mean μ	Standard deviation σ	COV	Max	Min
1	30	1.003	0.077	0.077	1.108	0.863
1.25	30	1.032	0.070	0.068	1.125	0.862
1.5	30	1.059	0.048	0.045	1.142	0.984
1.75	30	1.076	0.056	0.052	1.158	0.991
2	30	1.083	0.056	0.051	1.165	0.998
All	150	1.051	0.066	0.063	1.165	0.862

[34] combination. Within each b/h category, the mean value is found to be smaller than the mean value of the reduced combinations. Table 11 shows the minimum of the reduced local or global combination using imperfection proposed by Walport et al. [31]. Similar observations to that of the reduced combinations using imperfection proposed by Somodi et al. [34] can be made in this case.

Fig. 11 shows the ratio of the minimum of the studied combinations, reduced local or global combination (min($R_{eqv-SRL}$, $R_{eqv-SRG}$)), to the Somodi et al. [34] combination to show the slenderness range where the minimum of the reduced combination leads to overestimated results compared to the non-reduced Somodi et al. [34] combination. It is evident from the results that reducing one of the imperfections leads to a maximum increase in the resistance of approximately 6%. The largest overestimation occurs in the region of high global slenderness and low local slenderness for all b/h ratios.

4.4. Reliability assessment study

A reliability assessment study is conducted to show the applicability of the proposed combinations for the b/h ratios being studied. The study follows the guidelines specified in EN1990 Annex D [50] to examine the validity and accuracy of the proposed combinations. The details of the reliability assessment can be found in a previous study conducted by the authors focusing specifically on square box-section columns [24]. Here, only the final results are shown.

Table 12 shows the results of the reliability assessment, where the combination name, the applied global and local imperfections, the mean correction factor b, the coefficient of variation V_δ, the coefficient of

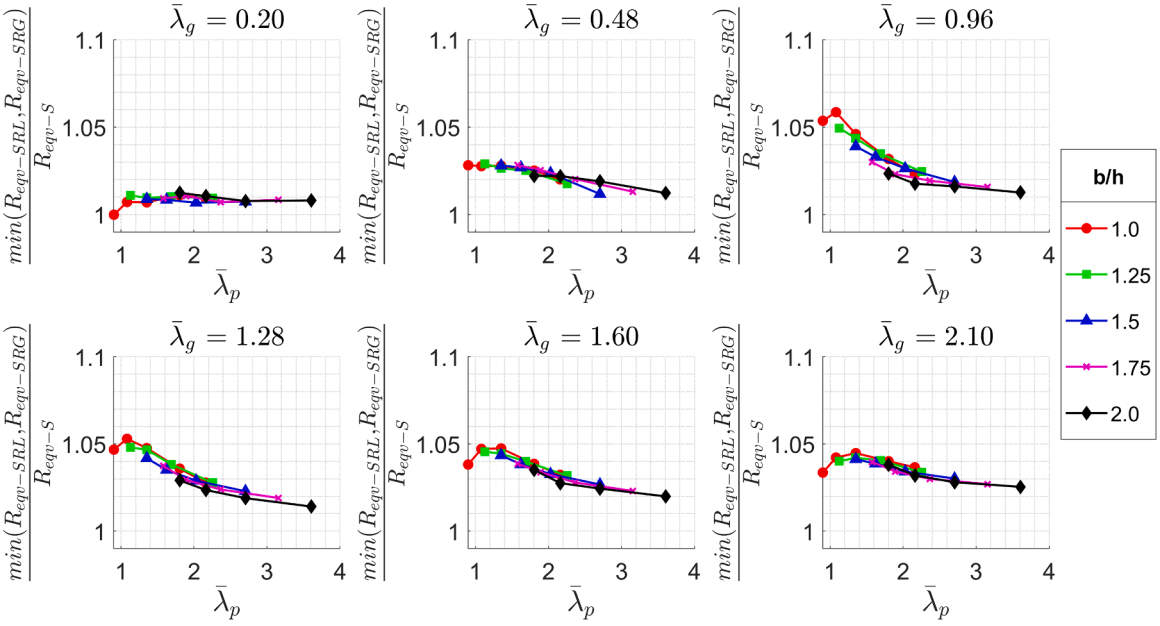

Fig. 11. Ratio of the minimum resistances (reduced local or global combination ($\mathbf{R_{eqv-SRL}}$, $\mathbf{R_{eqv-SRG}}$)) to the combination using 100% Somodi et al. [34] global imperfection and 100% local imperfection (b/125)(e.g. Somodi et al. [34] combination ($\mathbf{R_{eqv-S}}$)).

Table 12
Reliability assessment of the analysed combinations of imperfection.

Combination name	Global imp.	Local imp.	b	V_δ	V_{rt}	V_r	γ^*_M
Slenderness-dependant combination (SD)	Eq. (3)	Eq. (5)	1.11	0.080	0.086	0.117	0.93
SD-reduced global (SDRG)	0.7* Eq. (3)	Eq. (5)	1.07	0.058	0.086	0.104	0.99
SD-reduced local (SDRL)	Eq. (3)	0.7* Eq. (5)	1.05	0.069	0.086	0.110	1.07
Somodi et al. [34] combination (S)	Eq. (4)	b/125	1.05	0.084	0.086	0.121	1.12
Walport et al. [31] combination (W)	Eq. (1)	b/125	1.02	0.080	0.086	0.118	1.20
Somodi et al. [34] -Reduced local (SRL)	Eq. (4)	0.7* b/125	1.01	0.077	0.086	0.115	1.21
Somodi et al. [34] -Reduced global (SRG)	0.7* Eq. (4)	b/125	1.00	0.078	0.086	0.116	1.26
Walport et al. [31]-Reduced local (WRL)	Eq. (1)	0.7* b/125	0.99	0.073	0.086	0.113	1.30
Walport et al. [31]-Reduced global (WRG)	0.7* Eq. (1)	b/125	0.98	0.076	0.086	0.115	1.33

variation of the basic variables $V_{rt,}$ the coefficient of variation of the model V_r, and the corrected partial safety factor γ_M^*, for each combination are shown. The corrected partial safety factor is determined based on the nominal values of the basic variables and taking the effect of the overstrength factor of the steel material into consideration in the determination of γ_M^* [4,40]. The combinations are sorted in ascending order based on γ_M^* value. Based on the mean correction factor b, all the combinations provide safe results with a b value greater than 1.0 except for the reduced Walport et al. [31] combinations, where the b value is less than 1.0. If the uncertainties of the model and the basic variables are taken into consideration, the slenderness-dependant combinations provide the safest results with γ_M^* of 0.93. Furthermore, by decreasing the magnitudes of imperfections or applying a constant-value imperfection, the mean value approaches 1.0. However, due to the quite large standard deviation observed in the results, a relatively large γ_M^* is obtained.

5. Conclusion

Several researchers pointed out that equivalent geometrical imperfections specified in the Eurocode were originally developed for elastic analysis, raising questions about their applicability to GMNI analysis. Consequently, the authors conducted two parametric studies to derive equivalent global and local imperfection factors through a pre-existing database that incorporates accurate combinations of imperfections and residual stresses, which had been previously developed and researched by the authors [23]. These combinations showed good agreement with the experimental test results conducted on square box-sections. In the current research, parametric studies are performed on welded box-section columns made of S355 steel grade with different b/h ratios. A comparison is made to evaluate the buckling resistance of rectangular and square welded box-section columns. Furthermore, the applicability of the previously proposed imperfection combinations for square sections is examined for rectangular sections. Based on the numerical results, the following conclusions are drawn:

1. By using the accurate slenderness-dependant imperfections for both global and local buckling, results show that if the b/h ratio of the cross-section is increased, the application of the equivalent geometrical imperfections leads to a safe solution, which means that the equivalent geometric imperfections developed for square box-section columns can be safely utilised for rectangular section columns, as well.
2. By using the simplified, slenderness-independent imperfections for both global and local buckling, the following conclusions are drawn: (i) the buckling resistance for the $b/h = 1$ gives the upper-bound surface, meaning that the previously developed imperfections are safe for rectangular cross-sections; (ii) if the b/h ratio is increased, the ratio of the equivalent-to-accurate resistances will decrease; (iii) the ratio of the equivalent-to-accurate resistances exhibits an increasing trend with the increase of local slenderness ratio. As the local slenderness increases, the overestimation of the buckling resistance increases, as well and can reach up to 15% for large slenderness ratios ($\bar{\lambda}_{(p-b)} > 2$) due to applying a constant value for local imperfection (b/125). Thus, there are slightly unsafe resistances within the large slenderness region ($\bar{\lambda}_{(p-b)} > 2$), which rarely occurs in the design practice.
3. By using the 70% reduction rule for local and global imperfections, it is found that taking the minimum of the two imperfection combinations results in a mean value closer to the accurate solution and a smaller standard deviation compared to combinations with 100% magnitudes. However, numerical calculations show that reducing one imperfection to 70% only leads to small differences (max 6%) in buckling resistance. Nevertheless, the latter approach would double the computational efforts by performing the analysis twice.

CRediT authorship contribution statement

M. Radwan: Methodology, Software, Validation, Formal analysis, Investigation, Resources, Data curation, Writing – original draft, Writing – review & editing, Visualization. **B. Kövesdi:** Conceptualization, Methodology, Software, Validation, Formal analysis, Investigation, Resources, Data curation, Writing – review & editing, Visualization, Supervision, Project administration, Funding acquisition.

Declaration of Competing Interest

The authors declare that they have no known competing financial interests or personal relationships that could have appeared to influence the work reported in this paper.

Data Availability

Data will be made available on request.

Acknowledgement

The presented research program has been financially supported by the Grant MTA-BME Lendület LP2021-06/2021 "Theory of new generation steel bridges" program of the Hungarian Academy of Sciences and Stipendium Hungaricum Scholarship. Both grants are gratefully acknowledged.

References

[1] J. Shen, M.A. Wadee, Imperfection sensitivity of thin-walled rectangular hollow section struts susceptible to interactive buckling, Int. J. Non-Linear Mech. 99 (2018) 112–130, https://doi.org/10.1016/j.ijnonlinmec.2017.11.004.
[2] J. Shen, M.A. Wadee, Length effects on interactive buckling in thin-walled rectangular hollow section struts, Thin-Walled Struct. 128 (2018) 152–170, https://doi.org/10.1016/j.tws.2017.04.006.
[3] J. Shen, M.A. Wadee, A.J. Sadowski, Interactive buckling in long thin-walled rectangular hollow section struts, Int. J. Non-Linear Mech. 89 (2017) 43–58, https://doi.org/10.1016/j.ijnonlinmec.2016.11.007.
[4] N. Schillo, M. Feldmann, A. Taras, Local and Global Buckling of Box Columns Made of High Strength Steel, RWTH Aachen University, 2017.
[5] European Committee for Standardization (CEN), EN 1993-1-1:2005. Eurocode 3: design of steel structures - Part 1-1: general rules and rules for buildings, CEN, Brussels, 2005.
[6] A. van der Neut, The interaction of local buckling and column failure of thin-walled compression members, in: M. Hetényi, W.G. Vincenti (Eds.), Appl. Mech., Springer Berlin Heidelberg, Berlin, Heidelberg, 1969, pp. 389–399.
[7] K.J.R. Rasmussen, G.J. Hancock, Geometric imperfections in plated structures subject to interaction between buckling modes, Thin-Walled Struct. 6 (1988) 433–452, https://doi.org/10.1016/0263-8231(88)90012-2.
[8] B.W. Schafer, Local, Distortional, and Euler Buckling of Thin-Walled Columns, J. Struct. Eng. 128 (2002) 289–299, https://doi.org/10.1061/(ASCE)0733-9445(2002)128:3(289).
[9] B.W. Schafer, Review: the Direct Strength Method of cold-formed steel member design, J. Constr. Steel Res. 64 (2008) 766–778, https://doi.org/10.1016/j.jcsr.2008.01.022.
[10] J. Shen, M.A. Wadee, Local–global mode interaction in thin-walled inelastic rectangular hollow section struts part 2: assessment of existing design guidance and new recommendations, Thin-Walled Struct. 145 (2019), 106184, https://doi.org/10.1016/j.tws.2019.106184.
[11] J. Becque, K.J.R. Rasmussen, Experimental investigation of local-overall interaction buckling of stainless steel lipped channel columns, J. Constr. Steel Res. 65 (2009) 1677–1684, https://doi.org/10.1016/j.jcsr.2009.04.025.
[12] J. Becque, K.J.R. Rasmussen, A numerical investigation of local–overall interaction buckling of stainless steel lipped channel columns, J. Constr. Steel Res. 65 (2009) 1685–1693, https://doi.org/10.1016/j.jcsr.2009.04.027.
[13] X. Cao, R. Zhong, Y. Xu, C. Cheng, S. Liu, Z. Chen, S.E. Kim, Z. Kong, Local–overall interactive buckling behaviour of 800MPa high-strength steel welded H-section members under axial compression, Thin-Walled Struct. 164 (2021), 107793, https://doi.org/10.1016/j.tws.2021.107793.
[14] H.X. Yuan, Y.Q. Wang, L. Gardner, Y.J. Shi, Local–overall interactive buckling of welded stainless steel box section compression members, Eng. Struct. 67 (2014) 62–76, https://doi.org/10.1016/j.engstruct.2014.02.012.
[15] T. Usami, Y. Fukumoto, Welded box compression members, J. Struct. Eng. 110 (1984) 2457–2470, https://doi.org/10.1061/(ASCE)0733-9445(1984)110:10(2457).

[16] T. Usami, Y. Fukumoto, Local and overall buckling of welded box columns, J. Struct. Div. 108 (1982) 525–542, https://doi.org/10.1061/JSDEAG.0005901.
[17] S.P. Chiew, S.L. Lee, N.E. Shanmugam, Experimental study of thin-walled steel box columns, J. Struct. Eng. 113 (1987) 2208–2220, https://doi.org/10.1061/(ASCE)0733-9445(1987)113:10(2208).
[18] H. Degée, A. Detzel, U. Kuhlmann, Interaction of global and local buckling in welded RHS compression members, J. Constr. Steel Res. 64 (2008) 755–765, https://doi.org/10.1016/j.jcsr.2008.01.032.
[19] L. Pavlovčič, B. Froschmeier, U. Kuhlmann, D. Beg, Finite element simulation of slender thin-walled box columns by implementing real initial conditions, Adv. Eng. Softw. 44 (2012) 63–74, https://doi.org/10.1016/j.advengsoft.2011.05.036.
[20] Y.B. Kwon, E.G. Seo, Prediction of the compressive strength of welded RHS columns undergoing buckling interaction, Thin-Walled Struct. 68 (2013) 141–155, https://doi.org/10.1016/j.tws.2013.03.009.
[21] M. Khan, B. Uy, Z. Tao, F. Mashiri, Concentrically loaded slender square hollow and composite columns incorporating high strength properties, Eng. Struct. 131 (2017) 69–89, https://doi.org/10.1016/j.engstruct.2016.10.015.
[22] L. Yang, G. Shi, M. Zhao, W. Zhou, Research on interactive buckling behavior of welded steel box-section columns, Thin-Walled Struct. 115 (2017) 34–47, https://doi.org/10.1016/j.tws.2017.01.030.
[23] M. Radwan, B. Kövesdi, Improved design method for interaction buckling resistance of welded box-section columns, J. Constr. Steel Res. 194 (2022), 107334, https://doi.org/10.1016/j.jcsr.2022.107334.
[24] M. Radwan, B. Kövesdi, Equivalent geometrical imperfections for local and global interaction buckling of welded square box section columns, Structures 48 (2023) 1403–1419, https://doi.org/10.1016/j.istruc.2023.01.045.
[25] A. Müller, M. Vild, A. Taras, Decision tree for local + global imperfection combinations in double-symmetric prismatic members – Practical recommendations in the framework of advanced analysis, Steel Constr. 16 (2023) 2–15, https://doi.org/10.1002/stco.202200041.
[26] European Committee for Standardization (CEN), EN 1090-2: 2008+ A1: 2011. Execution of steel structures and aluminium structures-Technical requirements for steel structures, CEN, Brussels, 2011.
[27] European Committee for Standardization (CEN), EN 1090-2: 2018. Execution of steel structures and aluminium structures - Part 2: technical requirements for steel structures, CEN, Brussels, 2018.
[28] J. Jönsson, T.C. Stan, European column buckling curves and finite element modelling including high strength steels, J. Constr. Steel Res. 128 (2017) 136–151, https://doi.org/10.1016/j.jcsr.2016.08.013.
[29] J. Rondal, R. Maquoi, Le flambement des colonnes en acier, Chambre syndicale des fabricants de tubes d'acier (1980).
[30] European Committee for Standardization (CEN), prEN 1993-1-1:2019. Eurocode 3 – Design of steel structures – Part 1-1: general rules and rules for buildings., CEN, Brussels, 2019.
[31] F. Walport, L. Gardner, D.A. Nethercot, Equivalent bow imperfections for use in design by second order inelastic analysis, Structures 26 (2020) 670–685, https://doi.org/10.1016/j.istruc.2020.03.065.
[32] J. Lindner, U. Kuhlmann, F. Jörg, Initial bow imperfections e0 for the verification of flexural buckling according to eurocode 3 part 1-1 – additional considerations, Steel Constr. 11 (2018) 30–41, https://doi.org/10.1002/stco.201700013.
[33] J. Lindner, U. Kuhlmann, A. Just, Verification of flexural buckling according to Eurocode 3 part 1-1 using bow imperfections, Steel Constr. 9 (2016) 349–362, https://doi.org/10.1002/stco.201600004.
[34] B. Somodi, E. Bärnkopf, B. Kövesdi, Applicable equivalent bow imperfections in GMNIA for Eurocode buckling curves – SHS, RHS and welded box sections, J. Constr. Steel Res. 204 (2023), 107860, https://doi.org/10.1016/j.jcsr.2023.107860.
[35] European Committee for Standardization (CEN), EN 1993-1-5:2006. Eurocode 3: design of steel structures, Part 1.5: plated structural elements, CEN, Brussels, 2006.
[36] N. Schillo, A. Taras, M. Feldmann, Assessing the reliability of local buckling of plates for mild and high strength steels, J. Constr. Steel Res. 142 (2018) 86–98, https://doi.org/10.1016/j.jcsr.2017.12.001.
[37] M. Radwan, B. Kövesdi, Local plate buckling type imperfections for NSS and HSS welded box-section columns, Structures 34 (2021) 2628–2643, https://doi.org/10.1016/j.istruc.2021.09.011.
[38] M. Clarin, High Strength steel: Local Buckling and Residual Stresses, Luleå tekniska universitet, 2004.
[39] N. Schillo, M. Feldmann, Interaction of local and global buckling of box sections made of high strength steel, Thin-Walled Struct. 128 (2018) 126–140, https://doi.org/10.1016/j.tws.2017.07.009.
[40] M. Radwan, B. Kövesdi, Equivalent local imperfections for FEM-based design of welded box sections, J. Constr. Steel Res. 199 (2022), 107636, https://doi.org/10.1016/j.jcsr.2022.107636.
[41] British Standards Institution, BS EN 1090-2:2018. Execution of steel structures and aluminium structures. Technical requirements for steel structures, BSI, London, 2018.
[42] B. Johansson, R. Maquoi, G. Sedlacek, C. Müller, D. Beg, Commentary and worked examples to EN 1993-1-5 "plated structural elements, JRC Sci. Tech. Rep. (2007).
[43] ANSYS® v18, (2021).
[44] X. Yun, L. Gardner, Stress-strain curves for hot-rolled steels, J. Constr. Steel Res. 133 (2017) 36–46, https://doi.org/10.1016/j.jcsr.2017.01.024.
[45] European Committee for Standardization (CEN), prEN 1993-1-14:2020. Eurocode 3: design of steel structures, Part 1-14: design assisted by Finite element analysis (under development), CEN, Brussels, 2021.
[46] M. Khan, A. Paradowska, B. Uy, F. Mashiri, Z. Tao, Residual stresses in high strength steel welded box sections, J. Constr. Steel Res. 116 (2016) 55–64, https://doi.org/10.1016/j.jcsr.2015.08.033.
[47] Y.B. Wang, G.Q. Li, S.W. Chen, The assessment of residual stresses in welded high strength steel box sections, J. Constr. Steel Res. 76 (2012) 93–99, https://doi.org/10.1016/j.jcsr.2012.03.025.
[48] Y.B. Kwon, The development of the direct strength method for welded steel members with buckling interactions, Thin-Walled Struct 81 (2014) 121–131, https://doi.org/10.1016/j.tws.2013.07.016.
[49] L. Gardner, D. Nethercot, Numerical modeling of stainless steel structural components—A consistent approach, J. Struct. Eng. 130 (2004) 1586–1601, https://doi.org/10.1061/(ASCE)0733-9445(2004)130:10(1586).
[50] European Committee for Standardization (CEN), EN1990:2002. Eurocode—Basis of structural design, CEN, Brussels, 2002.